JOURNAL OF GEOPHYSICAL RESEARCH, VOL. 115, E04002, doi:10.1029/2009JE003490, 2010

A general circulation model ensemble study of the atmospheric circulation of Venus

C. Lee[1] and M. I. Richardson[2]

Received 10 August 2009; revised 16 October 2009; accepted 28 October 2009; published 1 April 2010.

[1] The response of three numerical model dynamical cores to Venus-like forcing and friction is described in this paper. Each dynamical core simulates a super-rotating atmospheric circulation with equatorial winds of 35 ± 10 m/s, maintained by horizontally propagating eddies leaving the equatorial region and inducing a momentum convergence there. We discuss the balance between the mean circulation and eddies with reference to the production of a super-rotating equatorial flow. The balance between the horizontal eddies and vertical eddies in the polar region is discussed and shown to produce an indirect overturning circulation above the jet. The indirect overturning may be related to the observed region of the polar dipole in the Venus atmosphere. Reservoirs of energy and momentum are calculated for each dynamical core and explicit sources and sinks are diagnosed from the general circulation model (GCM). The effect of a strong "sponge layer" damping to rest is compared with eddy damping and found to change significantly the momentum balance within the top "sponge layer" but does not significantly affect the super-rotation of the bulk of the atmosphere. The Lorenz (1955) energy cycle is calculated and the circulation is shown to be dominated by energy conversion between the mean potential energy and mean kinetic energy reservoirs, with barotropic energy conversion between the mean kinetic energy and eddy kinetic energy reservoirs. We suggest modifications to the GCM parameterizations on the basis of our analysis of the atmospheric circulation and discuss the effect of numerical parameterizations on the simulated atmosphere.

Citation: Lee, C., and M. I. Richardson (2010), A general circulation model ensemble study of the atmospheric circulation of Venus, *J. Geophys. Res.*, *115*, E04002, doi:10.1029/2009JE003490.

1. Introduction

[2] The atmosphere of Venus is observed to circumnavigate the planet at a much faster rate than the rotation of the underlying planet, resulting in a total atmospheric angular momentum that far exceeds that of a solid body rotation rate. This situation, known as super-rotation, is the subject of much research using general circulation models (GCMs), and a number of GCMs are able to simulate the super-rotating Venus atmosphere with some success [*Lee et al.*, 2007; *Yamamoto and Takahashi*, 2003; *Hollingsworth et al.*, 2006; *Herrnstein and Dowling*, 2007; *Lebonnois et al.*, 2008; *Parish et al.*, 2008]. However, these GCMs have been forced with variations on a set of simplified physical parameterizations (often "Newtonian relaxation" and "Rayleigh friction") that produces different atmospheric circulations. Since both the GCM and the physical forcing of these models are simultaneously varying in the studies, this complicates the analysis of the circulation and makes clean intercomparison of models difficult.

[3] One simple approach to this problem, used extensively when comparing GCMs in the terrestrial regime, is to force each GCM dynamical core with identical physical parameterizations (the "dynamical core" of a GCM is the component that solves the Navier–Stokes fluid equations under the boundary conditions prescribed by the physical parameterizations). *Held and Suarez* [1994] is an example of this, where a discrete grid dynamical core and a spectral dynamical core are subjected to the same forcing and friction schemes. Another, more complex, suite of tests is described by *Jablonowski and Williamson* [2006]. In this study, we use the physical parameterization described in detail by *Lee et al.* [2007] (hereafter LLR07) in order to simulate a super-rotating Venus-like atmosphere.

[4] For this study, we will use three dynamical cores from the Geophysical Fluid Dynamics Laboratory, Princeton, New Jersey (GFDL), Flexible Modeling System climate model [the GCM originally tested by *Held and Suarez*, 1994]. We will use the B grid core [*Arakawa and Lamb*, 1977], spectral core [*Held and Suarez*, 1994], and the finite volume (FV) core [*Lin*, 2004], each obtained from GFDL in the Memphis version of the GCM (the current public release version as of

[1]Division of Geological and Planetary Sciences, California Institute of Technology, Pasadena, California, USA.
[2]Ashima Research, Pasadena, California, USA.

0148-0227/10/2009JE003490

September 2009). As far as possible, we do not alter the dynamical cores.

[5] Although, the LLR07 parameterization is known to generate a super-rotating circulation under Venus-like conditions, it does not reproduce the observed wind speeds nor wave periods [e.g., *Del Genio and Rossow*, 1982, 1990; *Moissl et al.*, 2009]. One of the reasons for testing this parameterization with different numerical cores is to separate the components of the circulation, which are dependent on the physical parameterizations from the components that are artifacts of, or sensitive to, differences in numerical implementations of the dynamical cores.

[6] The forcing used here is also not the only one that could be used to test the dynamical cores with a super-rotating circulation. *Williams* [2003, 2006] developed a simplified parameterization that produces strong local super-rotation under terrestrial conditions, including fast planetary rotation rates. However, this parameterization was not used at the very low planetary rotation rate of Venus and it does not produce strong global super-rotation with a large globally integrated angular momentum as has been observed on Venus and simulated in modern GCMs [*Lee et al.*, 2007; *Yamamoto and Takahashi*, 2003].

[7] In the following section, we provide a brief description of the model-specific changes required to convert the three cores of the FMS Memphis GCM into a suitable GCM for this study. In section 3, we present and describe the state of the atmosphere at equilibrium and compare with results found in previous work using the same physical parameterizations [*Lee et al.*, 2007]. In section 4, we analyze the Lorenz energy cycle diagnostics [*Lorenz*, 1955; *Peixoto and Oort*, 1992] in the dynamical cores. In section 5, we examine the results of the experiments. Finally, in section 6, we provide a summary of our results.

2. Model Description

[8] We use the B grid core [*Wyman*, 1996; *Arakawa and Lamb*, 1977], spectral core [*Held and Suarez*, 1994], and the FV core [*Lin*, 2004] of the FMS GCM. In each case, we configure the dynamical core to have a horizontal resolution of approximately 5° degrees in both longitude and latitude (64×32 for the B grid and FV core, T21 for the spectral core), and a vertical resolution of about 3 km from the surface to 90 km, using the specified sigma coordinate levels given in LLR07. The thermal forcing, surface Rayleigh friction, and the top damping ("sponge layer") are also from LLR07.

[9] We use the horizontal diffusion/damping schemes available within each dynamical core. An eighth-order Laplacian diffusion scheme in the spectral core, a fourth-order diffusion scheme in the B grid core, and divergence damping in the FV core [e.g., see *Jacobson*, 1999]. In each model the diffusion/damping coefficient is set to be as small as possible to give reasonable results in line with LLR07, but no further "tuning" was made to exactly match that circulation. The diffusion time scale used is approximately 3 days for the spectral core and B grid core, and 1 day for the FV core. Unmodified Polar Fourier Filters are used in the B grid and FV grid to reduce grid-scale noise as the domain converges at each (physical and numerical) pole, with critical latitudes at 60° and 36°, respectively. No further explicit damping or diffusion is performed on the prognostic fields.

[10] The integration time step used in each dynamical core is as large as possible while maintaining numerical stability, but no attempt was made to maximize this value. The spectral core and B grid core use time steps of 120 s. The FV core uses time steps of 900 s. These numbers are somewhat below the absolute maximum stable time step for the GCM but there is no apparent sensitivity to shorter time step values.

[11] In each GCM configuration, results are output on 64 longitudinal and 32 latitudinal grid-points, either once every 10 days for long time scale analysis, or daily for diagnostic analysis at the end of an integration. Apart from the details given earlier, we retain the default values for all variables within the FMS dynamical cores. The values of physical constants are set according to LLR07 (i.e., gravitational acceleration, heat capacity, rotation rate, surface pressure are set to suitable values to simulate a Venus atmosphere).

[12] In addition to the setup described earlier, we ran the same experiment with a different sponge layer at the model top of each dynamical core. The original eddy damping term [*Lee et al.*, 2007] on the top layers of the model atmosphere is intended to reduce the effects of the "rigid lid" imposed by the fundamental numerical properties of the GCM and takes the form

$$\frac{\partial \chi}{\partial t} = -\frac{(\chi - \overline{\chi})}{\tau}, \tag{1}$$

where χ is the prognostic variable being damped, $\overline{\chi}$ is its longitudinal mean, and τ is the damping time scale. The damping is applied to the eddy field in order to minimize the energy lost through the model top. However, the conservative nature of the eddy damping with respect to angular momentum results in the transfer of eddy momentum from vertically propagating waves into the mean flow, producing a spurious jet within the damping region at the model top. The total angular momentum stored in this jet is small, but the low density of the tenuous atmosphere results in a fast jet.

[13] To test the effect of this damping on the circulation at the model top, we replace the eddy damping [eddy sponge layer, *Lee et al.*, 2007] with a damping of the full atmospheric field [*Yamamoto and Takahashi*, 2003, 2006, full sponge layer]. In the wind field, this is the same as setting $\overline{\chi}$ to 0 in equation (1), and causes mean and eddy energy to be removed from the GCM. In the temperature field, the sponge layer is disabled, instead the Newtonian relaxation (which is parameterized in the same way) is used with the relevant damping time scales, resulting in the removal of mean and eddy Available Potential Energy [*Lorenz*, 1955] from the system.

3. *Lee et al.*'s [2007] Experiment

[14] Using the setup described earlier, we integrated the six experiments (two experiments with each core) for 21,600 simulated Earth days (60 Earth years) and sampled days 21,600 to 22,599 of the each integration every 24 Earth hours (referred to here as the "diagnostic sample"). During

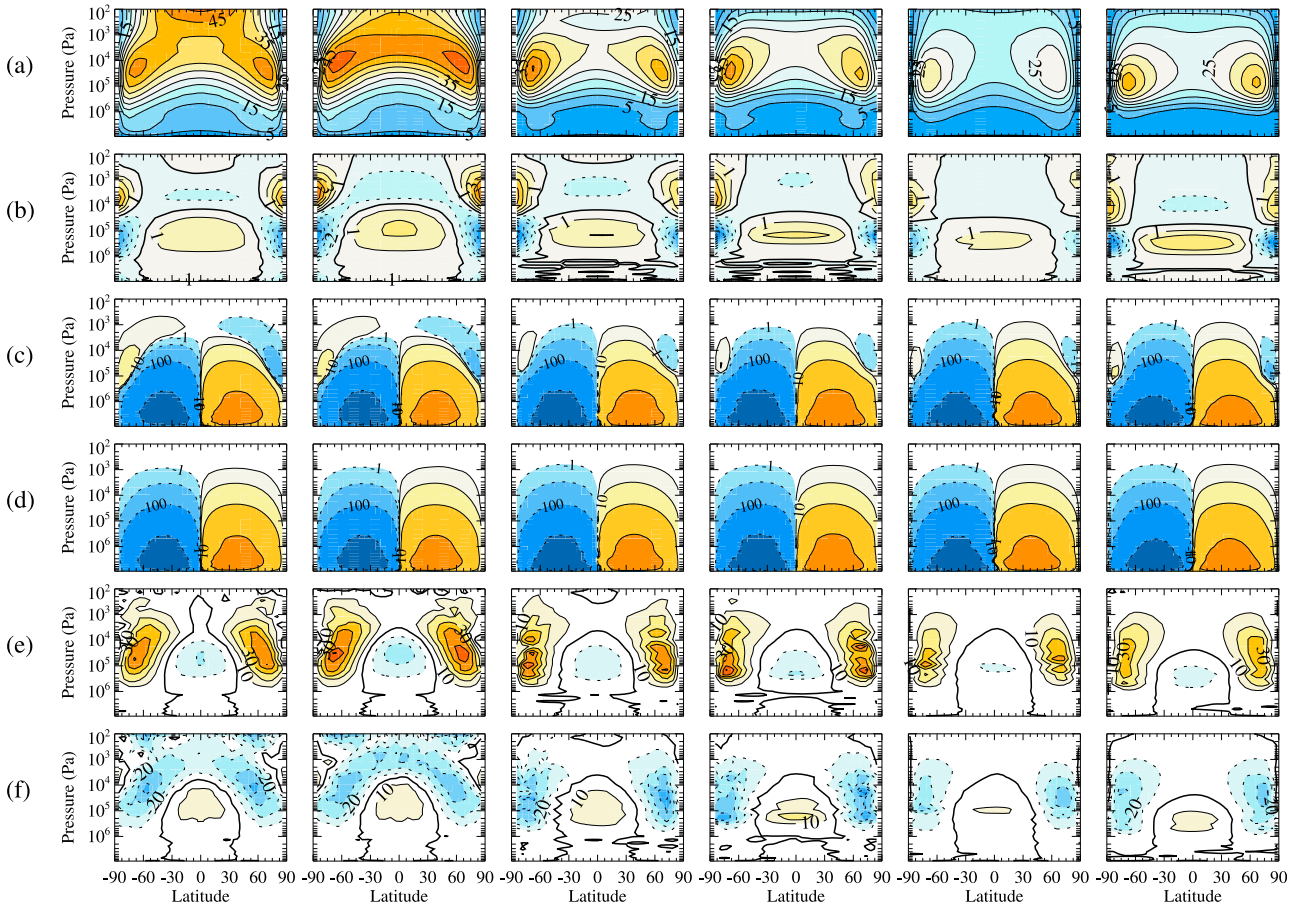

Figure 1. Diagnostics produced for the 1000 day diagnostic period for each experiment. The experiments run from left to right as (1) spectral core with eddy sponge layer, (2) spectral core with full sponge layer, (3) B grid core with eddy sponge layer, (4) B grid core with full sponge layer, (5) finite volume core with eddy sponge layer, and (6) finite volume core with full sponge layer. The diagnostic fields (all time and longitudinal means) are (a) westward wind (m/s), (b) mean temperature: global mean temperature profile ("temperature anomaly") (K), (c) Eulerian stream function (logarithmic contour interval, units of Tg/s), (d) transformed Eulerian mean stream function (logarithmic contour interval, units of Tg/s), (e) acceleration of the zonal wind due to the mean circulation (m/s^2), (f) acceleration of the zonal wind due to eddy convergence (m/s^2). Positive contours are shown by solid lines and negative contours are shown by broken lines.

the 1000 day diagnostic sample the variation in the potential energy is less that 0.01%, while kinetic energy and globally integrated super-rotation [*Read*, 1986a] vary by less than 3% (the total potential energy is (10^5) times larger than the total kinetic energy in this experiment). The peak time and longitudinal mean westward wind ($\overline{U}$) in the midlatitude jets is 48 m/s (±2 m/s over the ensemble of experiments) at about 67° ± 2° latitude at $10^{4.4\pm0.4}$ Pa (about 25 kPa), and 35 ± 10 m/s within the jets on the equator (4° ± 9° latitude) at $10^{3.5\pm0.7}$ Pa (about 3 kPa). The peak *instantaneous* winds within the jet in this experiment are 71 ± 3 m/s (at 69° ± 7° latitude at about $10^{4.1\pm0.2}$ Pa (about 12 kPa)). The wind speed appears reduced in the time and zonal mean because the peak winds are representative of the wave nature of the circulation, not the Eulerian mean circulation.

[15] Figure 1 shows diagnostics calculated for each dynamical core in this experiment. The diagnostics for these experiments are (from top to bottom in Figure 1): (1) the time and longitudinal mean of westward wind ($\overline{u}$); (2) the temperature anomaly ($\overline{T} - \overline{T(z)}$), used as a proxy for the available potential energy (APE); (3) the Eulerian; (4) transformed Eulerian mean (TEM) streamfunctions [*Andrews et al.*, 1987]; (5) the westward acceleration due to the mean circulation ($-u_\star \nabla m$ in the work of *Read* [1986a]); and (6) finally the westward acceleration due to Eliassen–Palm flux divergence ($-\nabla E$ in the work of *Read* [1986a]).

[16] The mean westward wind is calculated by taking the longitudinal and time mean of the entire 1000 days. The temperature anomaly is calculated by first calculating the time and longitudinal mean kinetic temperature, then subtracting the latitudinal average from this mean field. The stream functions are calculated as

$$\psi_m(\phi, P) = \frac{2\pi a \cos\phi}{g} \int_0^P [\overline{v}] dP, \qquad (2)$$

where ψ_m is the calculated stream function, a is the planetary radius (6.040×10^3 m), g is the gravitational acceleration

(8.87 m/s^2), P is the pressure, and ϕ is the latitude. For the Eulerian stream function $[\overline{v}]$ is the time and longitudinal mean meridional wind. For the TEM stream function $[\overline{v}]$ is replaced by $[\overline{v_\star}]$, the TEM residual meridional velocity, where

$$[\overline{v_\star}] = [\overline{v}] - \left[\frac{\overline{v'\theta'}}{[\overline{\theta_P}]}\right]_P, \quad (3)$$

and χ' is the longitudinal anomaly of χ, θ is the potential temperature [*Andrews et al.*, 1987], χ_P is the partial derivative of χ with respect to pressure ($\partial\chi/\partial P$). The TEM stream function is equivalent to the isentropic mass stream function [*Andrews et al.*, 1987].

[17] At altitudes below about 5 kPa, these fields have a similar structure to the circulation in LLR07. The westward jet peak forms near 70° latitude in both hemispheres, extending from 10 kPa to 1 MPa. In the lower atmosphere (about 500 kPa), the diabatic heating peak warms the equatorial air relative the polar air, producing a negative meridional temperature gradient (in the Northern Hemisphere) that drives the meridional overturning. In the upper atmosphere (about 5 kPa), the temperature gradient reverses with a (relatively) warm pole and (relatively) cold equator. The positive meridional gradient (in the Northern Hemisphere) is in agreement with a thermal wind balance where the jet begins to close, and the vertical gradient of u is negative [*Holton*, 2004].

[18] Both the wind and temperature fields in each experiment are also in reasonable agreement quantitatively with each other and LLR07. In the simulations shown here, the peak winds are around 40 m/s in the jets, as in LLR07, and the equatorial winds are 30–35 m/s, the warm equator at $10^{5.2\pm0.16}$ Pa (about 110 kPa) is 7.9 ± 1.2 K warmer than the pole at the same pressure, compared to 8 K warmer in LLR07. The warm pole at $10^{3.6\pm0.24}$ Pa (about 2.5 kPa) is 4.9 ± 1.2 K warmer than the equator at the same pressure, compared to 4 K in LLR07 (errors bars here indicate the standard deviation of each value over the ensemble).

[19] However, in the experiments with the eddy sponge layer shown here, the wind speed above 1 kPa is significantly larger than in the LLR07 GCM using similar damping. The top damping parameterization appears to be less effective in both the spectral core and the B grid core here than it was in the LLR07 GCM (a modified C grid HadCM3 core, developed by the United Kingdom Meteorological Office and modified by *Lee et al.* [2007]).

[20] The equatorial jet at the model top is a numerical artifact and suggests that either (1) the waves should damp lower in the atmosphere through a physical process, thus leading to a faster main westward jet, or (2) the model top should be transparent to the vertically propagating waves such that they do not damp at the model top and form the numerically driven jet.

[21] There is small region of surface eastward flow over the equator in this GCM (as in LLR07) as would be expected in order to balance the surface torque within the Rayleigh friction boundary layer scheme. This flow reversal is seen in other GCMs [e.g., *Herrnstein and Dowling*, 2007; *Yamamoto and Takahashi*, 2003], but this is not observed in the limited Pioneer Venus probe data [e.g., *Seiff*, 1983]. The lack of an observed flow reversal in the lower atmosphere of Venus suggests the planetary boundary layer may be more complicated than the simple one layer model allows here [e.g., *Monin and Obukhov*, 1954].

[22] There is some variation between each of the dynamical cores presented here. For example, the gross structure of the westward jet varies significantly between each of the dynamical cores and the type of numerical top-damping used. The temperature anomaly also varies between cores, but this variation is not independent of the jet structure as the two fields are related through the thermal wind relation.

[23] The large-scale features of the stream functions are similar in each of the dynamical cores and the LLR07 GCM. For comparison, the Eulerian stream function of the LLR07 GCM is shown in that paper, while the TEM stream function is shown in *Yung et al.* [2009]. Both the strength and extent of the equator-reaching stream function are similar in each of the dynamical cores. Importantly, each experiment replicates the large overturning circulation seen in the Eulerian stream function but not in the TEM stream function. This feature is dominated by the planetary scale Rossby waves in the polar regions and is only present between 1 MPa and 10 kPa, bounded approximately by the extrema of meridional temperature gradients.

[24] The spectral core may be producing the strongest circulation in the polar region because it has a better effective spatial resolution near the computational and physical poles. The spectral core uses a high-order horizontal diffusion and no polar filter, which results in a higher "effective" horizontal resolution in the polar region. The B grid and FV cores use polar filters to reduce numerical noise at the poles, resulting in smoother horizontal fields poleward of about 60°, which may reduce the wave activity associated with the overturning circulation in above and poleward of the jets. The resolution of the GCMs used here are insufficient to resolve finely (subdegree resolution) the polar structure observed in the atmosphere of Venus [e.g., *Taylor et al.*, 1980; *Irwin et al.*, 2008]. However, the location of this polar overturning cell relative to the westward jet, especially in comparison with those same features in observations [*Taylor et al.*, 1980], suggests that it is equivalent to the "polar dipole" in the Venus atmosphere.

[25] The accelerations due to the mean circulation and Eliassen–Palm flux divergence presented in Figure 1 are derived using the momentum evolution equation given in [*Read*, 1986a] as

$$m_t + u_\star \cdot \nabla m = -\nabla E + \frac{F}{\rho}, \quad (4)$$

where the terms are, in order, rate of change of momentum (m_t), deceleration due to the mean circulation ($u_\star \nabla m$), deceleration due to eddies (∇E) and the residual acceleration (F/ρ). Each term has units of m^2 s^{-2} (i.e., a rate of change in momentum). The residual acceleration term (F/ρ) includes contributions from viscosity in the GCM, either through sub grid-scale parameterizations of molecular viscosity or eddy viscosity (often parameterized using a numerical diffusion formulation), and contributions from parameterizations such as Rayleigh friction and the sponge layer. For relatively simple analytical models, the function form of F can be specified [*Read*, 1986b, 1986a].

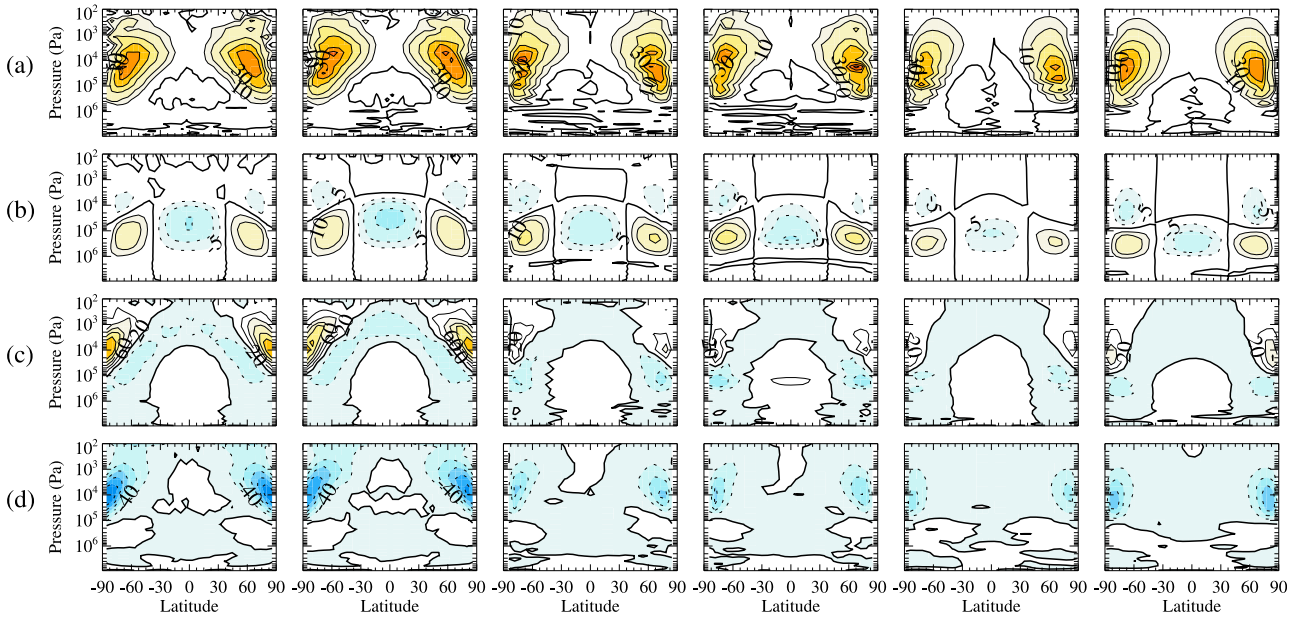

Figure 2. Diagnostics produced for the 1000 day diagnostic period for the same experiments as Figure 1. The diagnostics of acceleration of zonal wind due to (a) mean horizontal flow, (b) mean vertical flow, (c) eddy horizontal flow, and (d) eddy vertical flow are shown. All units are in m/s^2. Positive contours are shown by solid lines and negative contours are shown by broken lines.

[26] For the 1000 day diagnostic period, the first and last terms in equation (4) are negligible (both are <8% of either $u_\star \nabla m$ or $-\nabla E$ at any time for all pressures and latitudes outside of the sponge layer). As in LLR07, the mean overturning circulation tends to transport momentum from the equator to the midlatitudes, decelerating the equatorial jet while accelerating the midlatitude jets. Vertical transport (from the lower atmosphere) dominates in the equatorial region, while horizontal transport along the upper branch of the overturning circulation dominates at altitude (around 10 kPa) at all latitudes equatorward of the jet peaks. Eddies below the jet peaks tend to accelerate the equatorial flow while decelerating the midlatitude jets. The equilibrated circulation is a result of the balance between the accelerations due to the eddy activity and mean circulation in the atmosphere.

[27] Figure 2 shows the contribution of the horizontal and vertical components of the mean circulation and eddy fluxes to the acceleration of the westward flow for the experiments shown in Figure 1, represented by (1) acceleration by the mean horizontal circulation ($-v_\star(\partial m/\partial\phi)$), (2) acceleration by the mean vertical circulation ($-\omega_\star(\partial m/\partial P)$), (3) acceleration by the horizontal eddies ($-(1/R\cos\phi)(\partial E\cos\phi/\partial\phi)$), (4) acceleration by the vertical eddies ($-(1/R)(\partial E/\partial P)$).

[28] The momentum transport by the mean circulation is the classic picture of the Hadley cell (Figures 2a and 2b). Momentum is transported vertically upward at the equator and poleward in the upper branch of the overturning circulation, downward in the polar region and finally equatorward in the lower atmosphere. This overturning circulation causes a net deceleration of the westward wind in the equatorial region and a net acceleration in the midlatitude/polar region within the jets.

[29] The momentum transport by the eddies is more complicated. Below the westward jet peaks the equatorward momentum transport is dominated by the horizontal transport between the polar jets and the equatorial jet, causing a net acceleration of the equatorial winds and a net deceleration of the polar winds. Poleward and above the jet peaks, a large indirect cell is driven by the eddy activity, but there is very little net acceleration. The source of the waves may be barotropic instability, suggested by the presence of potential vorticity inflection points in the atmosphere [*Lee*, 2006]. However, *Iga and Matsuda* [2005] suggest that both Rossby and Rossby–Kelvin waves are able to grow in the presence of *shear instability* and transport momentum equatorward in the same way [*Yamamoto and Takahashi*, 2006].

[30] For the horizontal waves to transport momentum into the equator, the wave modes must satisfy the basic condition that the divergence of the horizontal EP flux is negative. This is analogous to the divergence of $-\overline{u'v'}$ being positive, or

$$-\frac{\partial\left(\overline{u'v'}\cos\phi\right)}{\partial\phi} > 0. \tag{5}$$

For example, if in the northern hemisphere $-\overline{u'v'}\cos\phi$ has a positive gradient, then $u'\cos\phi$ will tend to be negatively correlated with v', suggesting that meridional motions transport positive (i.e., westward, prograde with respect to the planet) perturbation angular momentum toward the equator.

[31] The negative momentum divergence itself suggests that the planetary/Rossby waves must propagate from the equator toward the polar jets. This may seem counterintuitive, as it is the equator that accelerates under the wave action described here. However, the momentum flux is

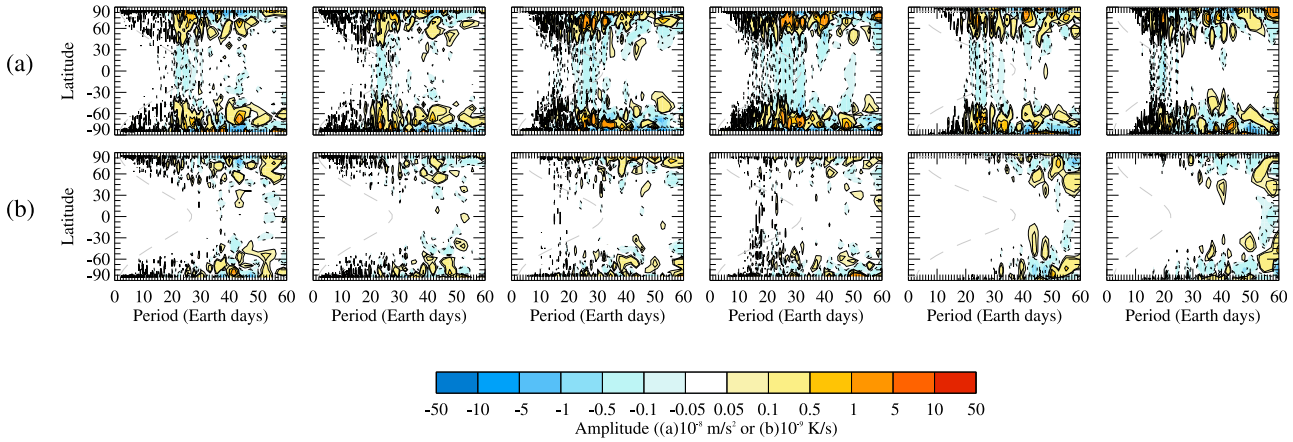

Figure 3. Diagnostics produced for the 1000 day diagnostic period for the same experiments as Figure 1. The divergence of the cross correlation at 150 kPa is shown between (a) u' and v', indicating deceleration due to the horizontal eddies (solid lines are deceleration, units of 10^{-8} m/s^2) and (b) v' and T', showing heating and cooling by the eddies (units of 10^{-9} K/s).

proportional to $-C_g^y$, where C_g^y is the meridional group velocity [*Andrews et al.*, 1987]. In order for the momentum flux to converge on the equator and accelerate the equatorial jet, the group velocity must be directed poleward (positive C_g^y). If the group velocity is directed poleward, then the *radiation condition* [*Vallis*, 2006] requires that the source of the Rossby waves exists on the equator [*Andrews et al.*, 1987; *Schneider and Liu*, 2009; *Saravanan*, 1993].

[32] Above and poleward of the jet peaks, horizontal EP flux convergence accelerates the westward wind, while vertical EP flux divergence decelerates it. The *net* acceleration from these contribution is small, but the activity there drives an indirect overturning circulation, like the Ferrel cell on Earth [*Holton*, 2004].

[33] The fact that horizontal momentum transport should dominate the super-rotation maintenance mechanism was first suggested by *Gierasch* [1975], and *Rossow and Williams* [1979] suggested that Rossby/MRG waves could be responsible under suitable conditions. These results are the same as found in LLR07 as well as other GCMs [*Yamamoto and Takahashi*, 2003; *Hollingsworth et al.*, 2006; *Herrnstein and Dowling*, 2007], where no diurnal cycle is forced.

[34] Equatorward momentum transport is dominated by the largest scale MRG/Rossby waves. In particular, wavenumber 1 westward propagating modes with a range of periods dominate both the momentum transport and the thermal energy transport. The net contribution from the remaining modes (up to Nyquist wavenumber) total less than 10% of the momentum and heat transported by the largest spatial mode. Figure 3 shows the divergence of the eddy momentum fluxes and eddy meridional heat fluxes at 150 kPa for the wavenumber 1 westward propagating modes. In the equatorial region, the momentum convergence (causing acceleration) peaks in eddies with a period of about 25 Earth days, with divergence (leading to deceleration) in the polar jets caused by eddies with the same period. The dominant wave period is almost the same as the effective period ($\tau_{\text{eff}} = 2\pi\ a\cos\phi/86{,}400\overline{u}\}$) of the mean westward wind on the equator, consistent with the suggested mechanism where equatorially generated waves are propagating poleward from their source region.

[35] There is some evidence for small amplitude Kelvin waves on the equator in these models, as in LLR07, with a shorter period than the mean flow over much of the atmosphere, and a smaller amplitude than the planetary waves. In order for these Kelvin waves to break efficiently within the atmosphere there must be a critical layer where the speed of the mean westward flow is faster than the propagation speed of the wave. In the models shown here, as in the LLR07 model, the Kelvin waves tend to propagate faster (longitudinally) than the mean flow everywhere and propagate to the model top without being significantly damped. The damping of these waves in the sponge layer may be the cause of the large equatorial jet at the model top seen in Figure 1.

4. Energy Cycle

[36] A complimentary method with which to analyze the equilibrated atmospheric state is to calculate the energy partitioning and energy conversions in the atmosphere. We diagnose the energy partitioning using two methods. We first calculate the energy reservoirs, generation, and dissipation terms using the explicit GCM diagnostics to diagnose the contributions from the physical parameterizations included in the GCM. We then calculate the energy cycle using the formulation pioneered by *Lorenz* [1955] and developed by *Peixoto and Oort* [1992, 1974].

[37] We explicitly output from each experiment the mean state of the atmosphere in the temperature and wind fields, and use these diagnostics to calculate the total potential energy (PE = $\langle C_p T\rangle$), Kinetic Energy (KE = $\langle \frac{1}{2}\vec{u}^2\rangle$), and angular momentum (AM = $\langle r\cos\phi(u + \Omega r\cos\phi)\rangle$) of the atmosphere. We also diagnose the rate of change of kinetic temperature and horizontal wind due to the Newtonian relaxation, Rayleigh Friction Planetary Boundary Layer (PBL), Top Damping sponge layer, and from these calculate the PE input ($\langle C_p \frac{\partial T}{\partial t}\rangle$), KE input ($\langle \overline{u}\frac{\partial \overline{u}}{\partial t}\rangle$), and momentum input ($\langle \frac{\partial u\cos\phi}{\partial t}\rangle$) where appropriate. In each term described above, $\langle\chi\rangle$ denotes a mass weighted volume integral of χ over the global domain. Table 1 lists each of these parameters for the experiments shown in Figure 1 and described in section 3.

Table 1. Energy Diagnostics Explicitly Calculated From the GCM Output[a]

	Spec Eddy	Spec Full	Grid Eddy	Grid Full	FV Eddy	FV Full
(a) PE	546.3	546.3	544.9	544.9	545.0	545.0
(b) KE	0.051	0.053	0.020	0.018	0.016	0.024
(c) AM	35.4	36.0	16.1	15.3	13.2	13.1
(d) ΔPE (Physics)	−9.6	−9.5	0.7	0.6	1.2	1.5
(d1) ΔPE (Newtonian relaxation)	−9.6	−9.6	0.7	0.6	1.2	1.5
(d2) ΔPE (top damping)	−1.57e−12	0.0	−1.94e−12	0.00e+00	−6.44e−13	0.00e+00
(e) ΔKE (physics)	−0.041	−0.046	−0.032	−0.033	−0.016	−0.017
(e1) ΔKE (Rayleigh friction)	−0.037	−0.040	−0.032	−0.033	−0.016	−0.017
(e2)ΔKE (top damping)	−3.36e-03	−6.08e-03	−2.02e-04	−3.70e-04	−1.05e-05	−1.05e-05
(f) ΔAM (physics)	8.87	3.95	41.6	43.8	57.7	65.7
(f1) ΔAM (top damping)	−9.76e-11	−0.84	6.14e-12	−0.07	−1.19e-11	−0.011
(f2) ΔAM (Rayleigh friction)	8.87	4.79	41.6	43.9	57.7	65.7

[a]PE, potential energy; KE, kinetic energy; AM, angular momentum; $\Delta\chi$, rate of change of χ. Reservoirs are given in GJ/m^2; rates (sources) are given in W/m^2.

[38] Even with identical physical parameterizations, the reservoirs and energy sources/sinks vary significantly between each core. The PE reservoir (a in Table 1) is approximately the same in each core, being dependent on the gross temperature structure that is highly stratified and stable for the simulated Venus atmosphere. The variation in the KE reservoir (b in Table 1) is because of differences in the lower atmosphere westward jets (altitudes below 1 MPa, 15–20 km), where the spectral core has a significant reservoir of KE containing 50% of its total KE reservoir.

[39] The PE input by the Newtonian relaxation (d1 in Table 1) is dependent on the relatively small deviations from the relaxed temperature profile, such that small differences in the anomaly temperature are exaggerated in the PE input in each experiment. At the rate of PE input calculated (d in Table 1) here, even for the FV core, the change in PE over the 1000 day diagnostic period is only 0.01%.

[40] The Rayleigh friction KE source/sink (e1 in Table 1) depends on the structure of the horizontal wind field at the surface. In each experiment, the meridional flow is equatorward everywhere with an eastward jet along the equator and westward jets in the midlatitudes. It is the magnitude of the westward jets that is most variable between cores, strongest in the spectral core and weakest in the FV core, and this is reflected in the source magnitudes; a larger westward surface flow leads to more deceleration and larger *sink*. The *momentum* (c in Table 1) source/sink in the PBL (f2 in Table 1) reflects the same results but with less variation between the experiments because the equatorial eastward jet dominates this field (because of the cosϕ term) and is similar in magnitude in each experiment.

[41] The PE sink due to the top damping sponge layer (d2 in Table 1) is insignificant. In the experiments that damp to zero, there is no explicit sponge PE sink (it is included in the Newtonian relaxation instead). In the experiments with the mean sponge layer, the formulation is essentially $\propto (\partial T/\partial\lambda)$ that should integrate to zero in a global integral. The small deviation from zero shown in Table 1 is because of the numerical approximations (discretization, grid conversion, etc.). The KE (e2 in Table 1) and momentum sink (f2 in Table 1) due to the sponge layer is more significant compared to the corresponding PBL sources/sinks (e1 and f1 in Table 1). The eddy sponge layer KE sink is 10% the size of the PBL sink, while the momentum sink is negligible (for the same reason as the PE sink above). The full sponge layer sinks about 20% of the PBL KE sink and 20% of the PBL momentum source.

[42] The sponge layer, therefore, does contribute to the overall energy balance within the GCM, but does not significantly affect the global structure of the equilibrated atmosphere. The full sponge layer might also increase the length of the "spin-up" phase of the integration relative to the eddy sponge because of the reduced net angular momentum input. It is unlikely that the full sponge layer will significantly affect the bulk of the circulation in an equilibrated simulation. In the experiments described here, the difference in circulation caused by the change of sponge layers was confined to the model top. The difference in globally integrated kinetic energy and momentum between GCM using the two sponge layer methods is <10% for both the B grid core and <5% for the spectral core.

[43] However, it is not clear that either sponge layer is more "correct" from a physical perspective. The eddy sponge not only reduces the numerical reflections from the rigid model top, but also causes additional damping at the model top. This has important implications for the upper atmosphere circulation in the wave-dominated circulation on Venus as the comparison of the eddy sponge with the full sponge experiments show. The full sponge layer is far more efficient at reducing the artifacts related to the equatorial jet produced by damping the eddies; however, it also implies that the velocities at the model top should be approximately zero in an equilibrated circulation. Both of these situations may be true to some extent in the Venus atmosphere, but probably not at 80 km.

[44] The performance of the FV core suggests a better sponge layer parameterization. In experiments without the explicit sponge layer (not shown), the divergence damping within the FV core was sufficient to reduce the noise at the model top and produce a circulation that was qualitatively similar to the explicitly damped experiments shown in Figure 1. Although, the divergence damping may be too strong in the bulk of the FV GCM (reducing the magnitude of the jet somewhat), it may be a useful method of reducing spurious reflections and circulations at the model top using a more realistic method than the "Rayleigh" damping used here.

[45] We also decompose the atmospheric state into reservoirs using the *Lorenz* [1955] formulation. This method gives us more detailed conversions of energy between the

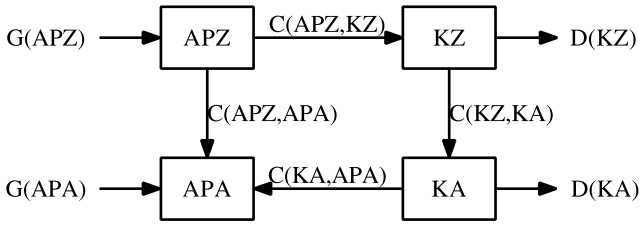

Figure 4. The Lorenz energy cycle calculated for this study. Each reservoir is shown as a box, each conversion is shown as an arrow between two reservoirs, and each generation term is shown as an arrow pointing to a reservoir (source) or from a reservoir (sink). APZ, zonal mean available potential energy; APA, eddy available potential energy; KZ, zonal mean kinetic energy; KA, eddy kinetic energy. $C(x,y)$ is conversion between reservoir x and reservoir y. $G(x)$ is generation of reservoir x. $D(y)$ is damping of reservoir y.

reservoirs, allowing us to build a more complete schematic of the energy "cycle" in that atmosphere.

[46] Using the methodology and terminology described by *Peixoto and Oort* [1974, 1992], we calculate reservoirs of APE (its mean denoted by APZ and eddy by APA), kinetic energy (KE, its mean KZ and eddy KA). We also calculate the resolved energy transfers between each of the four reservoirs, and the generating terms for available potential energy due to diabatic heating (through the Newtonian relaxation parameterization). A full description of each term is given by *Peixoto and Oort* [1992] [also *James*, 1994; *Holton*, 2004, and others). Figure 4 presents the Lorenz energy cycle that we analyze here. Reservoirs are contained in boxes, conversion terms $C(x, y)$, generation terms $G(x)$, and damping $D(x)$ are represented by arrows showing the direction of energy transfer. The diagnostics calculated for each dynamical core are shown in Figures 5a–5f.

[47] For each calculation, we show the time averaged and globally integrated values over the 1000 day diagnostic period, and retain one decimal place of precision. We have not corrected any imbalance produced by the calculation of each term independently. Any sources or sinks required to balance the energy cycle are added as parenthetical numbers with arrows indicating their assumed flow direction. Each reservoir is shown in units of 10^6 J/m^2 and each conversion, generation, and dissipation term in units of watt per square meter.

[48] The energy conversions in each of the dynamical cores are remarkably similar. Energy is initially supplied by diabatic heating as mean APE and converted through the zonally symmetric overturning into mean kinetic energy (APZ → KZ), accelerating the midlatitude jets. As shown in Figures 1c and 1d, this overturning is large and extends to the poles in part because of the slow planetary rotation [*Held and Hou*, 1980].

[49] Barotropic instabilities within the large westward jet drive energy transfer between the mean and eddy kinetic energy (KZ → KA). In doing so, planetary scale waves are generated in the equatorial region that propagate away from

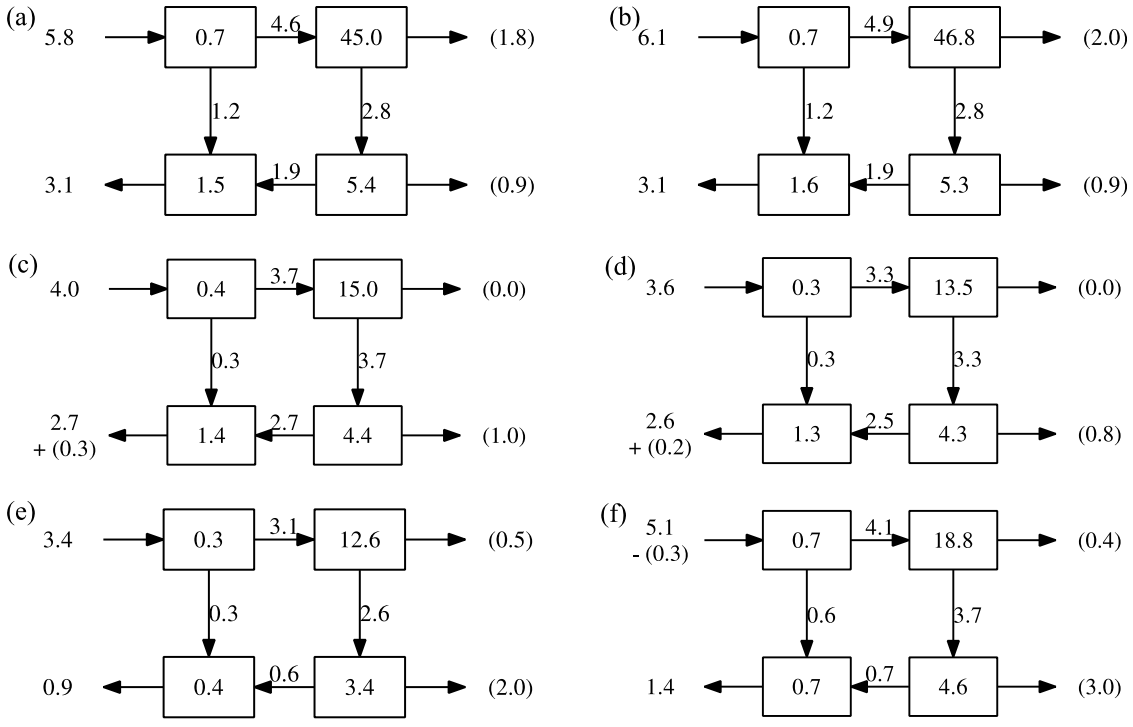

Figure 5. The atmospheric energy cycle calculated for (a) spectral core with eddy damping, (b) spectral core with full damping, (c) B grid core with eddy damping, (d) B grid core with full damping, (e) finite volume core with eddy damping, (f) finite volume core with eddy damping. Reservoirs (boxes) are shown as 10^6 J/m^2; conversions (lines) are shown as W/m^2. All numbers are stated as positive, with the arrow showing the direction of energy flow.

the equator and induce the observed equatorial super-rotation there as required by momentum and energy conservation.

[50] Energy is removed from the atmosphere in two ways, either through damping of the kinetic energy or through damping by the Newtonian relaxation (contained in G(APA)). The damping in the kinetic energy fields is explicitly diagnosed (listed in Table 1) for the specific physical parameterizations implemented for the Venus GCM, but not for the numerical parameterizations. However, the eddy sponge layer in the spectral model removes 0.003 W/m^2 of the Kinetic Energy (KA), while the PBL removes 0.037 W/m^2 from KA + KZ, leaving the majority of the kinetic energy sink (2.6 W/m^2) to be attributed to numerical process including diffusion, damping, or grid discretization. Note that, the PBL is not expected to be a significant source of kinetic energy in the system, most of which comes from the available potential energy through energy conversion (either APZ → KZ or APZ → APA → KA → KZ). More accurate diagnostics of the model internals would be required to constrain the sinks further, but this requires modification of the dynamical core code to allow the correct diagnostics to be made, and would increase significantly the computational cost of the integrations.

[51] The conversion process in these experiments is much different to the energy cycle present on faster rotating planets, such as the Earth [*Li et al.*, 2007], where the energy transfer between APZ and KZ is dominated by eddies, i.e., APZ → APA → KA → KZ. The energy cycle described above, i.e., APZ → KZ →KA → APA seems to occur only at the low rotation rates of Venus (and possibly Titan). This is true even when the physical forcing does not produce a globally super-rotating state [*Del Genio et al.*, 1993]. In a similar (more limited) analysis of the kinetic energy exchanges by *Yamamoto and Takahashi* [2006], energy flow is KZ → KA, again suggesting barotropic instabilities and probably APZ → KZ.

[52] The analysis of the energy cycle does not provide any explicit information on the super-rotation mechanism in the atmosphere. However, both the equatorward momentum transport and the KZ → KE energy conversions are dominated by the horizontal eddies ($\overline{u'v'}$). For example, it accounts for about 80% of the KZ → KE in the spectral core, and more than 90% of the EP flux convergence on the equator. The other experiments show similar results.

[53] The energy distribution between the reservoirs does suggest a reason for the relatively slow super-rotation in the experiments shown here and in *Lee et al.* [2007]. The process by which momentum is transferred into the equator limits the speed of the equatorial jet to be slower than or very close to midlatitude jets, otherwise momentum convergence would no longer occur on the equator, resulting in deceleration. A faster equatorial jet then requires a faster midlatitude jet and more mean kinetic energy (KZ) in the atmosphere. For the atmosphere to have more kinetic energy it must initially have more APE (either mean or eddy) or a more vigorous source of APE (G(PZ) or G(PA)), which is then converted through the atmospheric circulation into kinetic energy. Each of the equilibrated experiments have very little APE relative to KZ, suggesting that most of the APE → KZ conversion has already occurred, and that the sources and sinks are in statistical equilibrium.

[54] If the source of KE (supplied through the APE source) cannot be realistically larger, then the effective loss rate (D(KZ) and D(KA)) must be reduced. The loss rate through diffusive processes is dependent on the horizontal gradients in the wind field and a lower meridional gradient in $\overline{u}$ would tend to reduce these diffusive losses (Venus Express observed quite small gradients equatorward of 45°) [*Moissl et al.*, 2009]. However, some damping or diffusive processes are required to allow the wave-mean flow interaction that supplies momentum to the equatorial jet, maintaining the local super-rotation.

[55] Numerically, a faster jet could be obtained by modifying the Newtonian relaxation parameterization to enhance the peak latitudinal temperature gradient (increasing G(APE)) or decreasing the vertical extent of the peak heating (thus confining the jet in altitude). *Yamamoto and Takahashi* [2006] test the latter hypothesis and increasing the speed of the equatorial jet in their GCM from 100 to 120 m/s.

[56] *Lorenz* [1955] diagnostics suggest a source of available potential energy that is missing from the simulations because of the simplified forcing used. The eddy available potential energy generation term (G(APA)) is dependent on the correlation between temperature (T) eddies and diabatic heating (Q) eddies, e.g., from *Peixoto and Oort* [1992]

$$G(\mathrm{APA}) = \int \Gamma[T^{*}Q^{*}]dm, \tag{6}$$

where Γ is a stability factor [*Peixoto and Oort*, 1992]. The Newtonian Relaxation prescribed here and in *Lee et al.* [2007] provides no longitudinal variation in the solar forcing that may produce a positive correlation between T and Q. Instead, by prescription, the simplified Newtonian Relaxation produces a negative correlation between T and Q (the prescribed $Q \propto -T$). The APA generation provided by a diabatic heating with longitudinal structure may not result in a *net* generation of APA, but it would offset some of the losses through this term, thereby making more energy available to drive the atmospheric circulation and inducing faster westward winds. However, as shown in the experiments in this study, neither the diurnal thermal tides nor topographically driven waves are necessary to maintain some equatorial super-rotation if the instability generated MRG/Rossby waves are present. In experiments conducted by *Lee* [2006] and *Yamamoto and Takahashi* [2006], the diurnal thermal tides do not significantly *enhance* the equatorial super-rotation in the HadAM2-based Venus GCM, but the induced thermal tides do contribute to the momentum transport and equatorial super-rotation. In the experiment described by *Yamamoto and Takahashi* [2006], the diurnally varying forcing does increase the super-rotation, but detailed comparison is complicated by the changes in the mean Newtonian relaxation profile. In each of these experiments, and in similar experiments [*Lee et al.*, 2006] conducted with the NCAR WRF GCM [*Skamarock and Klemp*, 2008], thermally forced waves are present in the atmosphere and contribute significantly to the equatorward momentum transport.

5. Discussion

[57] The setup of the experiments described here was designed to limit the number of possible differences to those existing in the numerical cores themselves. Source-code

identical physical parameterizations were used for the Newtonian relaxation and Rayleigh friction schemes, and identical sponge layers were used in each of the dynamical cores.

[58] All three cores produce a suitable circulation when forced by the LLR07 parameterizations. All three GCMs simulate a super-rotating atmosphere with 35 ± 10 m/s equatorial winds, faster midlatitude jets, and an extended overturning circulation, as in the original experiments described in LLR07.

[59] The large scale circulation is similar in each GCM. Each dynamical core reproduces the westward jet at altitude with peak winds near 70° latitude and a slower equatorial super-rotating wind. The surface longitudinal winds of each GCM are eastward on the equator, westward in the polar region, and transition smoothly and monotonically between these two conditions. Meridional winds are equatorward in both hemispheres at the surface, and poleward at the top of the jets.

[60] The maintenance of the super-rotation is dominated by the same processes in each core. Horizontal eddies generated by Barotropic instabilities propagate away from the equator and induce a momentum convergence in the source region on the equator. In each experiment, the region of peak equatorial momentum convergence is located near the peak prescribed heating.

[61] In the polar region of each experiment, as in the LLR07 GCM, a secondary indirect overturning circulation is present. This Venusian "Ferrel" cell is trapped between the equatorial (Hadley like) cell and the poles, and is dominated by eddy divergence. It is located above the jet and does not reach the surface, being confined between the lower atmosphere "cold" polar region and the upper atmosphere "warm pole." The higher effective resolution (because of the higher order horizontal diffusion used) in the spectral core might allow it to simulate a stronger, better resolved, polar overturning circulation.

[62] The largest differences in the globally integrated diagnostics tend to be caused by differences in the lower atmosphere. Mass-weighted diagnostics are necessarily biased toward this region such that small differences in the horizontal wind field become large differences in the integrated kinetic energy reservoirs.

[63] The most significant numerical difference between the dynamical cores is the horizontal diffusion and damping parameterizations. The ∇^8 diffusion used in the spectral core has a lesser effect on the physical waves than the ∇^4 used in the B grid core and divergence damping used in the FV core. While it is clearly possible to reproduce the LLR07 Venus-like circulation with the latter damping schemes, the circulation is more sensitive to the numerical coefficients used in those dynamical cores.

[64] The sensitivity to the numerical choices within a dynamical core may be due to the simplification made in the physical parameterizations. For example, we do not explicitly force eddies (e.g., thermal tides) with the Newtonian relaxation, in order to investigate the simplest possible super-rotating atmosphere. However, the lack of eddy forcing may affect the eddy potential energy sink in a way that would not occur in the Venus atmosphere. A more realistic radiative parameterization could include the effect of the thermal tidal forcing and also allow for radiative interaction between atmospheric layers, something that is not possible with the linearized Newtonian relaxation. Unfortunately, it is difficult to prescribe a consistent forcing to allow interlayer radiative transfer without using a reasonably complete radiative transfer scheme. Such a parameterization would necessarily account for the effects of multiple scattering and high optical depth of the lower atmosphere.

[65] A more realistic radiative heating would additionally help clarify the radiative state of the lower atmosphere. *Hollingsworth et al.* [2006] suggest that the forcing used in *Yamamoto and Takahashi* [2003] and by similarity in *Lee et al.* [2007]) is unrealistically strong in the lower atmosphere, but *Yamamoto and Takahashi* [2006] show that it is difficult to produce the observed atmospheric circulation without an energy input greater than observed radiative forcing.

6. Summary

[66] We have implemented the forcing described by *Lee et al.* [2007] (hereafter LLR07) in three dynamical cores of the FMS GCM (the "Memphis" release) in order to produce a super-rotating atmospheric circulation under Venus-like conditions. The main purpose of this experiment was to investigate the sensitivity of the super-rotating circulation described in LLR07 to changes in the numerical parameterizations and more fundamentally to different numerical core choices.

[67] We have found that all three dynamical cores of the FMS GCM produce a super-rotating circulation using the forcing described in LLR07. The same momentum transport processes found there and in the work of *Yamamoto and Takahashi* [2003] dominate in the models used in this study. We find that there is little sensitivity within the dense atmosphere to changes in the top-damping "sponge layer." However, we do find that the simplified physical parameterizations of forcing and friction can lead to sensitivity to numerical parameterizations such as the type (order) of horizontal diffusion used.

[68] Simulating the atmosphere of Venus is the ultimate goal of this study, as such our experiments with simplified forcing using *multiple* dynamical cores has highlighted not only the need for improved parameterizations, but also the areas that would benefit from further investigation. Prior to this study, differences between the GCM and observations could be regarded as deficiencies in the particular GCM implementation. This is harder to assert with results from multiple GCMs, and the use of multiple dynamical cores will prove even more important in confirming the suitability of more complex parameterizations.

[69] We hope an outcome of this work is the beginnings of a comparison of circulation models in the Venus-like regime. A number of dynamical cores have been forced with the physical parameterizations prescribed by *Lee et al.* [2007], and most have reproduced the same circulation shown here (or at least exhibited the ability to do so). The baseline of results provided here can become a useful tool in diagnosing the problems found when GCMs are modified to extreme climates.

[70] **Acknowledgments.** The numerical simulations for this research were performed on Caltech's Division of Geological & Planetary Sciences Dell cluster. This work was performed under the NASA PATM grant

NNX07AF33G at the California Institute of Technology. We thank the two anonymous reviewers and the editor for their comments that have improved this manuscript.

References

Andrews, D. G., J. R. Holton, and C. B. Leovy (1987), *Middle Atmosphere Dynamics*, Academic, San Diego, La Jolla.

Arakawa, A., and V. R. Lamb (1977), Computational design of the basic dynamical processes of the UCLA General Circulation Model, *Meth. Comp. Phys.*, *17*, 173–265.

Del Genio, A. D., and W. B. Rossow (1982), Temporal variability of the ultraviolet cloud features in the Venus stratosphere, *Icarus*, *51*, 391–415.

Del Genio, A. D., and W. B. Rossow (1990), Planetary-scale waves and the cyclic nature of cloud top dynamics on Venus, *J. Atmos. Sci.*, *47*, 293–318.

Del Genio, A. D., W. Zhou, and T. P. Eichler (1993), Equatorial superrotation in a slowly rotating GCM: Implications for Titan and Venus, *Icarus*, *101*, 1–17.

Gierasch, P. J. (1975), Meridional circulation and the maintenance of the Venus atmospheric rotation, *J. Atmos. Sci.*, *32*, 1038–1044.

Held, I. M., and A. Y. Hou (1980), Nonlinear axially symmetric circulations in a nearly inviscid atmosphere, *J. Atmos. Sci.*, *37*, 515–533.

Held, I. M., and M. J. Suarez (1994), A proposal for the intercomparison of the dynamical cores of atmospheric general-circulation models, *Bull. Am. Met. Soc*, *75*(10), 1825–1830.

Herrnstein, A., and T. E. Dowling (2007), Effects of topography on the spinup of a Venus atmospheric model, *J. Geophys. Res.*, *112*, E04S08, doi:10.1029/2006JE002804.

Hollingsworth, J., R. Young, G. Schubert, C. Covey, and A. Grossman (2006), A simple-physics global circulation model for Venus: sensitivity assessments of atmospheric superrotation, *Geophys. Res. Lett.*, *34*, L05202, doi:10.1029/2006GL028567.

Holton, J. R. (2004), *An Introduction to Dynamic Meteorology*, 4th ed., Elsevier, San Diego, La Jolla.

Iga, S. I., and Y. Matsuda (2005), Shear instability in a shallow water model with implications for Venus atmosphere, *J. Atmos. Sci*, *62*, 2514–2527.

Irwin, P. G. J., R. de.Kok., A. Negrao, C. C. C. Tsang, C. F. Wilson, P. Drossart, G. Piccioni, D. Grassi, and F. W. Taylor (2008), Spatial variability of carbon monoxide in Venus' mesosphere from Venus express/visible and infrared thermal imaging spectrometer measurements, *J. Geophys. Res.*, *113*, E00B01, doi:10.1029/2008JE003093.

Jablonowski, C., and D. L. Williamson (2006), A baroclinic instability test case for atmospheric model dynamical cores, *Quart. J. R. Meteorol. Soc.*, *132*(621), 2943–2975.

Jacobson, M. Z. (1999), *Fundamentals of Atmospheric Modeling*, Cambridge Univ. Press, Cambridge, U. K.

James, I. N. (1994), *Introduction to Circulating Atmospheres*, Cambridge Univ. Press, Cambridge, U. K.

Lebonnois, S., F. Hourdin, A. Crespin, V. Eymet, R. Fournier, and J.-L. Dufresne (2008), Modelling Venus' atmospheric mean meridional circulation: sensitivity to radiative transfer scheme and to specific heat, *EGU General Assembly*, *10*, Abstract EGU2008-A-03909.

Lee, C. (2006), Modelling of the Atmosphere of Venus, Ph.D. thesis, Univ. of Oxford, Oxford, U. K.

Lee, C., M. I. Richardson, C. E. Newman, and A. D. Toigo (2006), Venuswrf: A new Venus GCM using PlanetWRF, *Eos Trans. AGU*, *87*(52), Fall Meet. Suppl., Abstract P51B-1202.

Lee, C., S. R. Lewis, and P. L. Read (2007), Superrotation in a Venus GCM, *J. Geophys. Res.*, *112*, E04S11, doi:10.1029/2006JE002874.

Li, L. M., A. P. Ingersoll, X. Jiang, D. Feldman, and Y. L. Yung (2007), Lorenz energy cycle of the global atmosphere based on reanalysis datasets, *Geophys. Res. Lett.*, *34*, L16813, doi:10.1029/2007GL029985.

Lin, S.-J. (2004), A "vertically Lagrangian" finite-volume dynamical core of global models, *Mon. Weather Rev.*, *132*, 2293–2307.

Lorenz, E. N. (1955), Available potential energy and the maintenance of the general circulation, *Tellus*, *7*, 157–167.

Moissl, R., et al. (2009), Venus cloud top winds from tracking UV features in Venus monitoring camera images, *J. Geophys. Res.*, *114*, E00B31, doi:10.1029/2008JE003117.

Monin, A. S., and A. M. Obukhov (1954), Basic laws of turbulent mixing in the ground layer of the atmosphere, *Trans. Geophys. Inst. Akad. Nuak.*, *151*, 1963–1987.

Parish, H. F., G. Schubert, C. C. Covey, and A. Grossman (2008), Simulation of Venus atmospheric dynamics with an earth climate gcm, *Eos Trans. AGU*, *89*(53), Fall Meet. Suppl., Abstract U23E–0092.

Peixoto, J. P., and A. H. Oort (1974), The annual distribution of atmospheric energy on a planetary scale, *J. Geophys. Res.*, *79*, 2149–2159.

Peixoto, J. P., and A. H. Oort (1992), *Physics of Climate*, AIP, Melville, N. Y.

Read, P. L. (1986a), Super-rotation and diffusion of axial angular momentum: 1. A review of quasi-axisymmetrical models of planetary atmospheres, *Quart. J. R. Met. Soc.*, *112*(471), 253–272.

Read, P. L. (1986b), Super-rotation and diffusion of axial angular momentum: 2. "speed limits" for axisymmetrical flow in a rotating cylindrical fluid annulus, *Quart. J. R. Met. Soc.*, *112*(471), 231–252.

Rossow, W. B., and G. P. Williams (1979), Large-scale motion in the Venus stratosphere, *J. Atmos. Sci.*, *36*, 377–389.

Saravanan, R. (1993), Equatorial superrotation and maintenance of the general circulation in two-level models, *J. Atmos. Sci*, *50*, 1211–1227.

Schneider, T., and J. J. Liu (2009), Formation of jets and equatorial superrotation on Jupiter, *J. Atmos. Sci.*, *66*, 579–601.

Seiff, A. (1983), Thermal structure of the atmosphere of Venus, in *Venus*, edited by D. M. Hunten et al., pp. 215–279, Univ. of Ariz. Press, Tucson.

Skamarock, W. C., and J. B. Klemp (2008), A time-split nonhydrostatic atmospheric model for weather research and forecasting applications, *J. Comp. Phys.*, *227*(7), 3465–3485.

Taylor, F. W., et al. (1980), Structure and Meteorology of the Middle Atmosphere of Venus: Infrared Remote Sensing From the Pioneer Orbiter, *J. Geophys. Res.*, *85*, 7963–8006.

Vallis, G. K. (2006), *Atmospheric and Oceanic Fluid Dynamics*, Cambridge Univ. Press, Cambridge, U. K.

Williams, G. P. (2003), Barotropic instability and equatorial superrotation, *J. Atmos. Sci.*, *60*, 2136–2152.

Williams, G. P. (2006), Equatorial superrotation and barotropic instability: Static stability variants, *J. Atmos. Sci.*, *63*, 1548–1557.

Wyman, B. (1996), A step-mountain coordinate general circulation model: Description and validation of medium-range forecasts, *Mon. Weather Rev.*, *124*, 102–121.

Yamamoto, M., and M. Takahashi (2003), The fully developed superrotation simulated by a general circulation model of a Venus-like atmosphere, *J. Atmos. Sci.*, *60*, 561–574.

Yamamoto, M., and M. Takahashi (2006), Superrotation maintained by meridional circulation and waves in a Venus-like AGCM, *J. Atmos. Sci.*, *63*, 3296–3314.

Yung, Y. L., M. C. Liang, X. Jiang, S. R. L., C. Lee, B. Bezard, and E. Marcq (2009), Evidence for OCS conversion to CO in the lower atmosphere of Venus, *J. Geophys. Res.*, *114*, E00B34, doi:10.1029/2008JE003094.

C. Lee, Department of Geological and Planetary Sciences, California Institute of Technology, M/C 150-21, 1200 East California Blvd., Pasadena, CA 91125, USA. (lee@gps.caltech.edu)

M. I. Richardson, Ashima Research, Pasadena, CA 91109, USA.